A computational analysis of the interaction of lattice and intramolecular vibrational modes in crystalline α-RDX

Sylke G. Boyd[a] and Kevin J. Boyd
Division of Science and Mathematics, University of Minnesota-Morris, Morris, Minnesota 56267, USA

(Received 30 June 2008; accepted 28 August 2008)

The vibrational spectrum of a computer model of crystalline RDX was studied using a 216-molecule periodic supercell, allowing for intra- and intermolecular degrees of freedom using the force field by Boyd *et al.* [J. Chem. Phys. **124**, 104508 (2006)]. The normal modes were analyzed with regard to their activity involving molecule center-of-mass translations and rotations, as well as 15 intramolecular degrees of freedom, including bond stretches, bend and dihedral angle variations, and out-of-plane motions of the nitro groups. We correlate center-of-mass motions with the occupation of internal degrees of freedom for all of the normal modes in the model with particular attention to correlations between nitro rotations and lattice modes. Transfer of lattice energy to internal degrees of freedom can occur through doorway modes and is significant for the initiation of detonation. Several clusters of potential doorway modes are found which involve significant lattice motion as well as nitro rotations. Such groups of modes have been found in the ranges between 186 and 220 and between 420 and 434 cm^{-1}. Symmetry properties and details of the involved molecular motions are described. © *2008 American Institute of Physics*. [DOI: 10.1063/1.2987368]

I. INTRODUCTION

The mechanisms leading to detonation initiation in high-energetic explosives, such as RDX, have been a matter of some debate. The role of hot spots, possibly centered at defects in the crystal geometry, has been pointed out.[1–3] These are regions of strong activity concentrated around defect sites or grain boundaries. These hot spots have been associated with the initial bond breaking during the beginning of a detonation. Even with these irregularities in the crystal matrix, the mechanism of the first bond breaking incident must involve a transfer of energy to intramolecular degrees of freedom. The search for such a transfer mechanism of energy from lattice motions, such as one may find in a Shockwave, to internal degrees of freedom leads one to consider the possible role of coupled vibrational modes between the lattice vibrations and molecular eigenmodes.[4–7] The search for evidence of so-called doorway modes,[4,8] which may facilitate such an energy transfer, has spawned several experimental studies of the vibrational spectra of RDX using Raman[5,6,9] and IR (Refs. 9–12) spectroscopies. Another motivation for the increased interest in the vibrational properties of high explosives lies in the possibility of unobtrusive detection using terahertz spectroscopy.[13] The frequency region of interest would coincide with the location of doorway modes and uses the IR signature in this region. Computer models have been developed which allow to study the influence of shock on the electronic properties[14] and defect behaviors[15,16] as well as the behavior of the materials under various thermodynamic conditions.[17–22] The experimental spectra of the free molecule and crystalline RDX cannot be mapped onto each other directly due to symmetry reduction in the crystal[6] and the presence of lattice modes. Data from polarized spectroscopy allow conclusions about the symmetry of certain modes; however, there is uncertainty about the actual motions incurred. The interpretation of experimental spectra often can greatly be aided by computer models.[5,6] In order for a computer model to be able to contribute to our understanding of the vibrational properties of these molecular crystals, it appears to be essential that the model not only can describe the molecule itself at sufficiently high accuracy but also is able to embed the molecule within the crystalline environment. The vibrational spectrum of the crystal needs to be analyzed using both intra- and intermolecular degrees of freedom if our interest is in finding vibrational modes that allow for resonances between lattice vibrations and molecular modes.

In this paper, we use the force field of Boyd *et al.*[23] in order to study various aspects of the vibrational properties of crystalline RDX. By using a large periodic model of α-RDX for the calculation of its normal modes, we can show that the frequencies of primarily molecular modes within the crystal are shifted to higher frequencies. The phonons were analyzed with respect to their symmetry within the D_{2h} factor group in order to facilitate comparison to the Raman data of Haycraft *et al.*[6] We also analyze the normal modes with regard to their effective projections on various degrees of freedom in the system. For example, we can isolate the fractional contributions to molecular center-of-mass (c.m.) rotations and translations as well as to molecule-internal degrees of freedom, such as bonds or bending angles. Under the presumption that a potential doorway mode must exhibit significant c.m. translations as well as intramolecular motions, we have searched for correlations between the lattice character of the normal modes and their engagement in internal degrees of freedom. Three clusters of modes have been identified, in which significant nitro motion is accompanied by molecular c.m.

[a]Author to whom correspondence should be addressed. Electronic mail: sboyd@morris.umn.edu. Tel.: 320-589-6315.

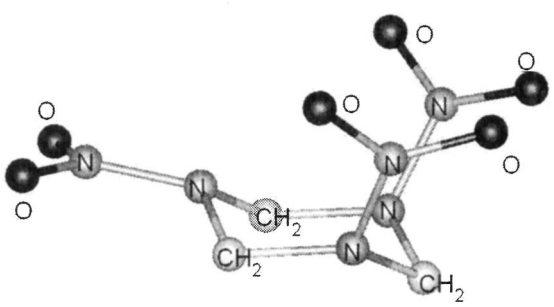

FIG. 1. The *Caae* conformer of the RDX molecule.

movement. Two of these clusters are located at 186–214 and 214–220 cm^{-1}, respectively. These two clusters correspond to twist motions of the ring structure of the molecule, with the more massive nitro groups essentially staying in place. One further band between 420 and 434 cm^{-1} exhibits the desired properties as well and corresponds to the symmetric methylene wagging modes. If modes in these clusters engage, they ultimately would allow transfer of energy from lattice to internal degrees of freedom. In particular, the lower two clusters of modes are likely candidates for doorway modes since they involve significant dihedral distortions of the nitro groups around the N–N bond. One of the proposed reaction path ways for detonation is the initial splitting of the three N–N bonds, and it is feasible that our lower proposed band may facilitate such a first step. Our model does not allow to follow this reaction, and it is quite possible that defects play a role in engaging these modes particularly strongly, corresponding to a focusing effect. The calculations have become possible due to two major developments: (i) the use of a force field which includes flexible molecules while accurately describing the intermolecular interactions and (ii) the availability of distributed computing capacity. All simulations were performed on a 32-node Linux cluster and use a computer code specifically developed for this purpose.

The sections below cover the computational methodology, a brief comparison between the normal mode spectra of free molecule conformers and the crystal model, an analysis of the normal mode spectrum of α-RDX (in particular, of the engagement of various degrees of freedom for various clusters of modes) and a summary of results.

II. COMPUTATIONAL MODEL

The RDX molecule can have various conformations. The ring can be present as a chair (C), boat (B) or twist (T) conformer. We found the chair conformation to be the energetically stable form, followed by a twist conformation as a metastable conformation. Furthermore, the three nitro groups may present an axial (a) or equatorial (e) orientation with respect to the normal vector of the ring. Figure 1 shows a schematic of the *Caae* conformer of the molecule, which is the conformation found in the most common crystalline form, α-RDX.[24] In the vapor phase, the molecule transits into C_{3v} symmetry, corresponding to the *Caaa* conformation.[25] The elementary cell of α-RDX contains eight molecules in *Pbca* symmetry. The molecular mechanics force field used for these calculations was published in Ref. 23. The force field includes intramolecular as well as intermolecular terms and allows for flexible molecules while giving satisfying treatment to long-range Coulomb and van der Waals interactions. Those long-range terms were subject to a smooth cutoff function in the range of 15 Å. It is noteworthy that the intermolecular components of this force field had been fitted for a variety of properties of the molecular crystal of α-RDX, including correct reproduction of symmetry and geometry. It performed satisfactorily for a variety of benchmarks, such as bulk modulus and expansion coefficients. The basic crystalline system has been modeled as $3\times3\times3$ primitive cells, corresponding to 216 molecules. This corresponds to 4536 atoms within a periodic supercell of $38.702\,05\times33.500\,71\times32.114\,53$ $Å^3$. For energy minimization, a conjugate gradient procedure with a cutoff criterion of a minimum force has been applied. An Andersen–Berendsen scheme was employed for temperature and pressure control. The annealing procedure allowed the system to adjust the box size as well as possible conformation changes. With a pressure of 1 atm and an initial temperature of 400 K, the system was annealed at an approximate rate of 3 K/ps. At a temperature of 50 K, the annealing was stopped, and the system relaxed into its nearest energetic minimum configuration. The normal mode analysis was then performed for this system, yielding 13 608 normal modes.

The solution of the eigenvalue problem

$$(A-\lambda_i)\vec{X}_i=0$$

yields eigenvalues $\lambda_i=m_i\omega_i^2$ as well as vibrational eigenvectors $\vec{X}_i$. The diagonalization of the Hessian matrix A is based on the Householder algorithm using distributed processors. The Hessian matrix was approximated by differential force calculations associated with small displacements of 0.01 Å for each degree of freedom. The eigenvectors $\vec{X}_i$ are of the dimension of a length and provide amplitude information for three directions of motion for each particle in the system. The goal is to find doorway modes which would engage intra- as well as intermolecular degrees of freedom.

The following procedures have been applied to identify lattice and molecular portions of modes: Lattice modes involving the translation of molecules are identified by a net amplitude of molecules as a whole. The c.m. translation of molecule j in mode i is given as

$$\vec{a}_{ij}=\sum_{k=1}^{21}\vec{X}_{ijk}.$$

Index k runs over all particles in one molecule. These molecular translations are then combined into a net translational character T_i of lattice mode i as

$$T_i=\sum_j|\vec{a}_{ij}|. \quad (1)$$

Lattice modes may contain portions involved in rotation of whole molecules around their c.m. For molecule j in mode i, the net rotation can be calculated as

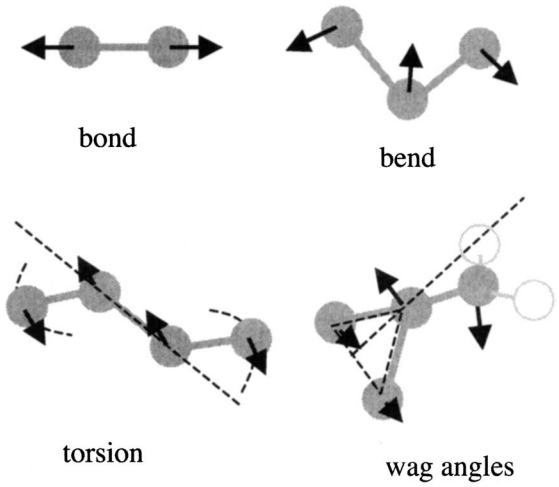

FIG. 2. Sketch of characteristic directions for the internal motions of the molecule.

$$\vec{b}_{ij} = \sum_{k=1}^{21} (\vec{r}_{\text{c.m.},k} \times \vec{X}_{ijk}).$$

These are combined as

$$R_t = \sum_j |\vec{b}_{ij}| \qquad (2)$$

in order to define the net rotational character of a lattice mode. These vibrational contributions correspond to the optical and possibly acoustical modes of the lattice. In addition to the c.m. motion of a molecule, normal modes may involve characteristic intramolecular motions, such as bond stretches, bending motions, torsional rotations, as well as wag motions of the nitro side group. Those active directions typically are the same as the direction of the force of the particular type of motion which are routinely calculated in a molecular mechanics force field. Hence, one can project the eigenvector onto the typical directions of motion, and thus find a fractional contribution of a mode to certain internal degrees of freedom. For example, the characteristic direction of a bond stretch motion would be defined by a vector $\vec{r}_{ij}$ from atom i to atom j. For this bond to stretch (or compress), atom i would move in the $\vec{r}_{ij}$ $(-\vec{r}_{ij})$ direction, while atom j will shift in the $-\vec{r}_{ij}$ $(\vec{r}_{ij})$ direction. The active directions for bonds, bends, torsions, and out-of-plane motions are sketched in Fig. 2. The activity of 15 internal motions has been considered, including CN, NN, CH, and NO bonds, CNC, NCN, CNN, NCH, NNO, ONO, and HCH bends, CNCN, NCNC, and CNNO torsions, and (CNC)–N wag angle of the nitro groups. If $\vec{f}_{lm}$ is the active direction for particle m in a group of type l, then the net activity of this group in the crystalline system can be calculated as

$$A_{il} = \sum_m (\vec{f}_{lm} \cdot \vec{X}_{ilm})^2 \qquad (3)$$

for the vibrational eigenmodes i and internal motions of type l. The summation is over all particles in the system as relevant for motion type l. This activity will become large if a particular normal mode involves motions of type l, and thus provides us with the ability to analyze the contributions of intramolecular degrees of freedom to the normal modes of the crystal. The modes were analyzed for their symmetry within the D_{2h} factor group as well.

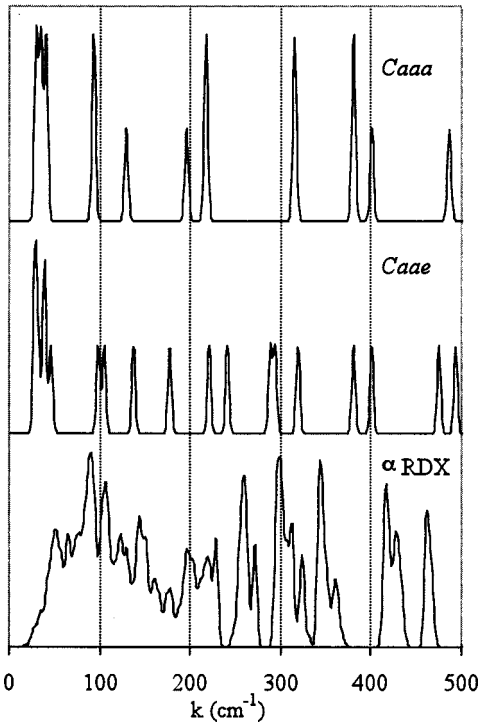

FIG. 3. Low-wave-number range of the normal mode density of states of *Caaa* and *Caae* conformers, as well as crystalline α-RDX at a pressure of 1 atm.

All frequency discussions below refer to the values found with the force field of Agrawal *et al.*[17] While the positions of some intramolecular modes are not perfectly aligned with the experimental findings, the force field was fitted to the bulk crystal properties of RDX and has a surprisingly good agreement in the low-frequency range with the few experimental references for the range.[6,12]

III. RESULTS AND DISCUSSION

We have identified the vibrational modes for the *Caae* conformer within the framework of our model in Ref. 23. Comparisons to other computational and experimental findings are described there as well. Below, we focus on the crystalline system of α-RDX and reference only a few details of the single-molecule calculations. The normal mode spectra for the *Caaa* and *Caae* conformers as well as for the ideal RDX crystal at a pressure of 1 atm are shown in Figs. 3–6. The figures of the spectrum were broken up into four wave number intervals in order to be able to show more detail. Tables I and II list the central location of groups of modes found for the crystalline system and give information with regard to the particular motions involved.

A. Comparison of free molecule and crystalline system

The crystalline normal modes were calculated for a 216-molecule system, shown in the bottom panel of Figs. 3–6.

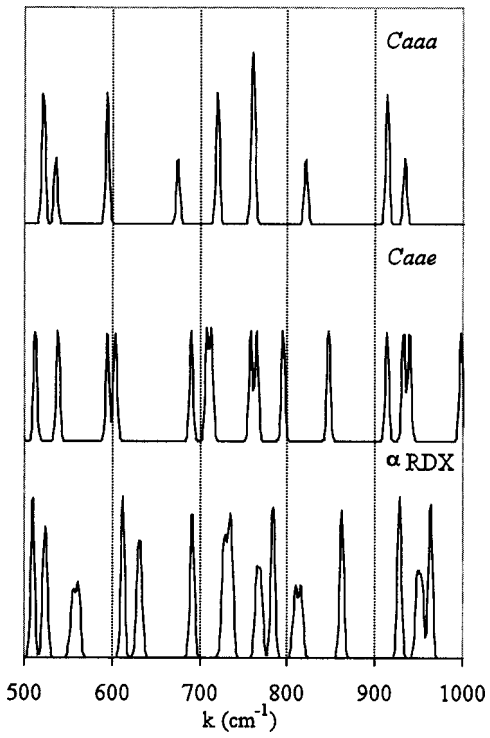

FIG. 4. Lower medium range of the normal mode density of states of *Caaa* and *Caae* conformers, as was as crystalline α-RDX at a pressure of 1 atm.

The normal mode spectra of the two isolated conformers are very similar. The dominating difference is found in the splitting of degenerate modes in the *Caae* conformer due to the loss of symmetry. An example is the splitting of the modes

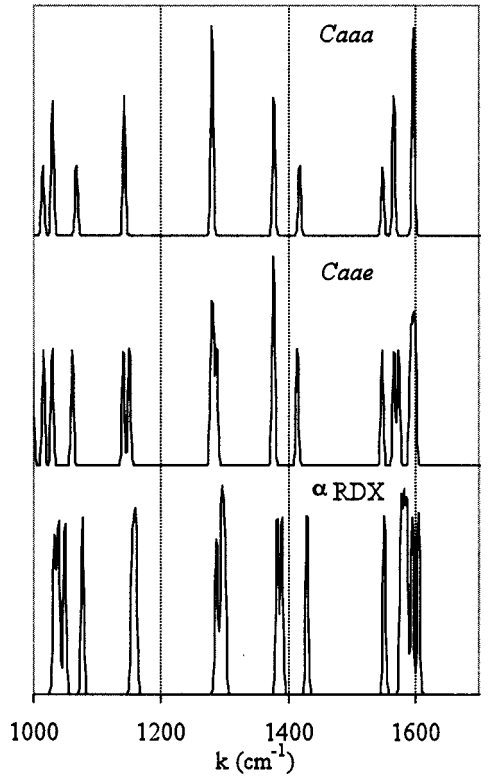

FIG. 5. Upper medium range of the normal mode density of states of *Caaa* and *Caae* conformers, as well as crystalline α-RDX at pressure of 1 atm.

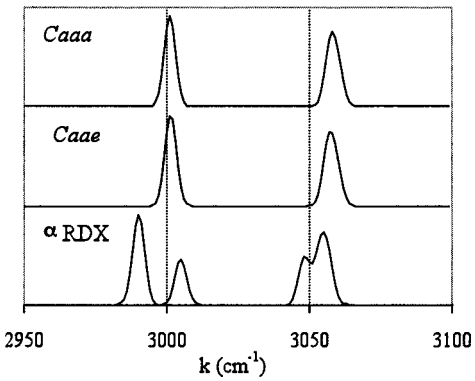

FIG. 6. High-range of the normal mode density of states of *Caaa* and *Caae* conformers, as well as crystalline α-RDX at a pressure of 1 atm.

centered at 598 and 603 cm^{-1}. This particular mode corresponds to combinations of NO_2 scissor motions and CH_2 wagging. In the crystalline material, these same modes are observed at 609 cm^{-1}. The region of the spectrum associated with the hydrogen stretch modes shows no noticeable difference between the conformers of the free molecule; symmetry restrictions in the crystal lead to a splitting of both the symmetric stretch modes around 3000 cm^{-1} and the asymmetric stretch modes around 3050 cm^{-1}. There are multiple features of the normal mode spectrum worth noting compared to the free molecule. The low-frequency range (0–500 cm^{-1}) includes optical lattice modes. The low-frequency boundary is settled by the size of the supercell used in the calculations but would be more populated if a larger system was considered. As concisely explained by Haycraft *et al.*,[6] symmetry considerations result in a dissolution of the fingerprints of individual molecules, in particular, in the low region where the constraints of crystal symmetry and the respective molecule symmetry yield sets of modes which cannot be found in the same form in isolated molecules. It is worth noting, again, that while the exact location of the calculated normal modes differs slightly from experimental values, the use of the same force field for all three of the eigenvalue analyses ensures that any differences between the spectra arise indeed from the behavior of the system as a crystal. The modes of the free *Caae* conformer between 28 and 46 cm^{-1} correspond to wagging and torsional motions of rigid nitro groups. These types of modes are absorbed into the large group of mostly lattice modes between 79 and 150 cm^{-1}. The spatial constraints in the crystal do demand modification of such motions. In the medium range of frequencies between 500 and 1700 cm^{-1}, see Figs. 4 and 5, the three spectra become more similar again. Modes observed for the free molecule shift to higher frequencies in the crystal. One may obtain some splitting of degenerate levels for some of the CH_2 rocking modes around 1400 cm^{-1}. Focusing on the high-frequency end of the spectrum, shown in Fig. 6, we find that the hydrogen stretch modes have shifted relative to the situation in the free molecule. The structure of resonance frequencies found in the crystalline model aligns perfectly with the experimental Raman observations in this range.[5,6]

Tables I and II include references to Raman experimental results of Haycraft *et al.*[6] The alignment with the normal

TABLE I. Centers of bands (0–1000 cm^{-1}) calculated from the normal modes of this model arranged by wave number and symmetry. The intensities are based on the density of states for the particular mode group (vw, very weak; w, weak; m, medium; s, strong; vs, very strong). Alignment with Raman results of Haycraft *et al.* (Ref. 6) based on wave number and intensity. Potential doorway modes are in boldface.

Normal modes, this paper							Raman-active modes, Haycraft *et al.* (Ref. 6)			
A_g	B_{1g}	B_{2g}	B_{3g}		Dominant degrees of freedom	Description	A_g	B_{1g}	B_{2g}	B_{3g}
22	25	24	25	vw	c.m. trans,[b] c.m. rot	Lattice modes	21.8	20.2	18.9	20.5
31	31	32	31	vw			29.4	29.2	18	37.4
41	41	40	41	w			38.8	43.8	40	49
49	49	50	49	m			49.6	49.9	48.5	54.6
66	65	65	66	s			59.5	57.9	59.1	58.7
79	80	79	80	m	c.m. rot, c.m. trans, CNNO	Lattice modes with	71.9	69.2	73	71
89	88	88	89	m		some NO_2 rotations	90	90.1	87.1	87.7
101	102	101	100	m			107.3	105.6	106	105.9
116	115	115	115	w						
128	128	129	129	m			129.5	127	129	130.6
142	140	142	141	m			139	139.9	138.9	143.6
155	156	156	154	w			150.3	149.5	148.2	150.2
166	163	164	161	w						
175	175	175	171	w						
190	192	190	190	m		NO_2 rotations				
201	198	202	199	m	CNNO, c.m. trans, c.m. rot	Ring rotation around	207.5	206.8	206.6	204.8
212	213	213	212	w		ring normal				
223	222	223	224	m	c.m. trans (CNNO)	Ring rotation around in-plane axis				
255	255	254	254	s	CNNO, CNCH (CNCN, NNO)	Torsional modes of the	225.4	226.4	225	225.2
269	268	268	269	w		nitro group				
297	297	296	296	vs			299.6	298.6	300.4	298.4
310	310	309	309	m						
321	321	321	320	m						
341	342	342	341	s	CNCN, CNCH, CNNO, CNC,	Ring modes	344.8	345.8	346	344.6
356	357	357	357	m	CNN, NNO					
414	413	413	414	m			414.8	414.8	414.4	414
426	425	425	425	m	c.m. trans, CNCH, CNNO, CNCN	CH_2 wag				
461	461	461	461	m	CNCH (CNNO, OOP)	Ring modes	464	463.2	461.8	463
							484	483.2	483	483
507	507	507	507	m	NNO	NO_2 rocking and ring	493	492	492	493
521	521	521	521	m		modes				
555	555	555	555	s			591.3	590	590.4	590.2
609	609	609	609	m	ONO (CNCH, CNCN, NCN)	NO_2 scissor and ring	606.2	606	604.8	605.2
628	628	628	628	m		mode combinations				
689	688	689	688	m			670.7	668.4	669.6	667.4
729	729	729	729	vs	NCH, CNCH	CH_2 wagging mode	885	884.4	883.2	883.8
762	762	762	762	w	ONO	NO_2 scissor				
767	767	767	767	vw						
781	781	781	781	m	NCH, CNNO, CNCN	CH2 wagging modes	787.4	787.6	786.2	786.6
806	806	805	805	w						
813	813	812	813	w						
							847.5	846.6	846.6	847.4
859	859	859	859	m	CNC, NCN, CNCH, OOP (CNNO)	Ring modes	857.7	857.2	857.4	857.4
925	925	925	925	m	NCH, CNCH	CH_2 twist modes				
946	946	946	945	w	CNCN					
952	951	950	951	w						
961	961	961	961	m			942.9	944.6	942.6	942.8

[a] Raman analysis of α-RDX, combination bands omitted.
[b] c.m. trans, c.m. translations; c.m. rot, c.m. rotations of molecules.

AQ: #3

modes received in our calculations is based on two factors: wave number and intensity. We assigned intensities to the normal modes using the density of states in the particular bracket of the spectrum. There are discrepancies between the normal mode spectrum and the experimental Raman spectrum. In particular, two areas are affected by these: The CH_2 twist motions (1036–1073 cm^{-1}) as well as the CH_2 wagging modes (729 and 781–813 cm^{-1}); both are governed by torsional force field parts. However, in examining the low-frequency parts of the spectrum we find excellent agreement

TABLE II. Centers of bands (above 1000 cm^{-1}) calculated from the normal modes of this model arranged by wave number and symmetry. The intensities are based on the density of states for the particular mode group (vw, very weak; w, weal; m, medium; s, strong; vs, very strong). Alignment with Raman results of Haycraft *et al.* (Ref. 6) based on wave number and intensity.

Normal modes, this paper							Raman-active modes, Haycraft *et al.* (Ref. 6)			
A_g	B_{1g}	B_{2g}	B_{3g}		Dominant degrees of freedom	Description	A_g	B_{1g}	B_{2g}	B_{3g}
1029	1030	1030	1030	m	NCH (NNO)	CH_2 rocking modes	1031.7	1030.8	1030.6	1029.6
1036	1036	1036	1036	m	NCH, CNC, CNCH	CH_2 twist modes				
1046	1046	1046	1046	m						
1073	1073	1073	1073	m						
1152	1152	1152	1152	m	HCH, NCH, CNCH	CH_2 scissor modes				
1157	1157	1157	1157	m						
							1217	1216.4	1215.9	1215.1
1284	1284	1284	1284	m			1273.2	1270.6	1273.8	1271.3
1294	1295	1295	1295	s			1311.4	1309.4	1311	1310.2
1379	1380	1380	1380	m	CN, NCH, CNCN	CH_2 rocking modes	1376.8	1376.2	1377.2	1377
1387	1387	1387	1387	m			1388.8	1390	1389.8	1386.4
1426	1427	1426	1426	m			1435.9	1435.6	1435.8	1435
					NO, NN	NN and NO stretch	1458.4		1459.4	1461.4
1548	1548	1548	1548	m		modes	1541.1	1541.4	1540.2	1540.8
1575	1574	1575	1574	m			1569	1569.8	1571.4	1571.6
1579	1579	1579	1579	m						
1584	1584	1584	1584	m	NO, NN, CN	Asymmetric NO stretch				
1593	1593	1593	1593	m			1594	1594.6	1594.4	1594
1602	1602	1602	1602	m			1596.3	⋯	1599.2	1600
2987	2987	2987	2987	s	CH	Symmetric CH stretch	2949.5	2947.6	2948.6	2948.2
3002	3002	3002	3002	m			3002.7	3002	3001.8	3001.8
3045	3045	3045	3045	m		Asymmetric CH stretch	3068.5	3067.6	3067.8	3066.8
3052	3052	3052	3052	vs			3077.3	3075.6	3077.8	3076.8

[a] Raman analysis of α-RDX; combination bands omitted.
[b] c.m. trans, c.m. translations; c.m. rot, c.m. rotations of molecules.

in placement as well as intensity of the normal mode groups, supporting the meaningfulness of the intermolecular force field as well as encouraging further inquiry as to the possibility of modes with lattice and molecular components.

B. Analysis of eigenmode spectrum of α-RDX

An analysis of the fractional contributions of various characteristic motions in the system to the normal has been performed, as outlined in the previous section. Figures 7–11 do show the activity of all 15 internal degrees of freedom as well as of c.m. translations and rotations of whole molecules for the normal modes. This analysis allows us to pinpoint whether a group of normal modes involves significant lattice motions or by which intramolecular degrees of freedom it may be dominated.

In Fig. 7, the contributions of the eigenvectors to the four types of bond stretch motions have been isolated. Bond stretch motions contribute only at very sharply defined frequencies. Those frequencies are nearly identical to the ones found for the free molecule. N–O and N–N stretches are found at nearly identical frequencies around 1584–1602 cm^{-1}. The region of the CH stretches around 3000 cm^{-1} is not shown, and these bonds do not contribute to any other modes in the lower range. The CH_2 rocking modes at 1379–1426 cm^{-1} are associated with the C–N stretch modes.

The contributions to the seven types of bend angle motions shown in Figs. 8 and 9 split into two wave number intervals. The CH_2 scissor motions around 1152–1295 cm^{-1} are the only feature involving this bend angle. The NCH bend angle contributes to a wide variety of modes between

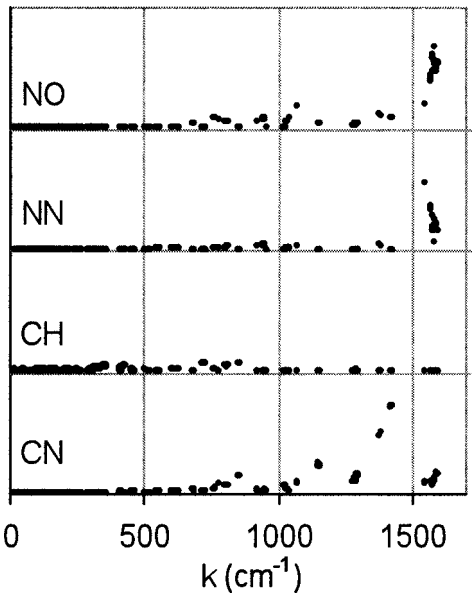

FIG. 7. Activities of bond stretches in the normal mode spectrum of the crystal. The CH range around 3000 cm^{-1} is omitted.

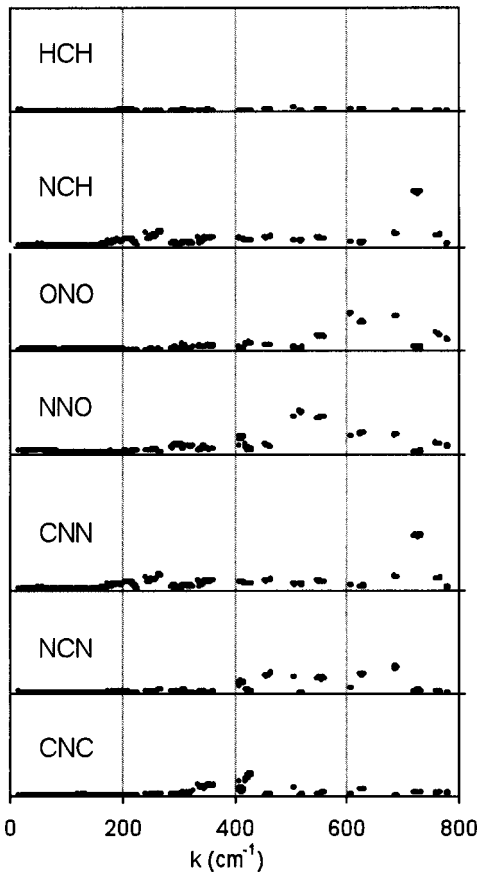

FIG. 8. Activities of bend angles in the normal modes of the crystal, wave number range from 0 to 800 cm^{-1}.

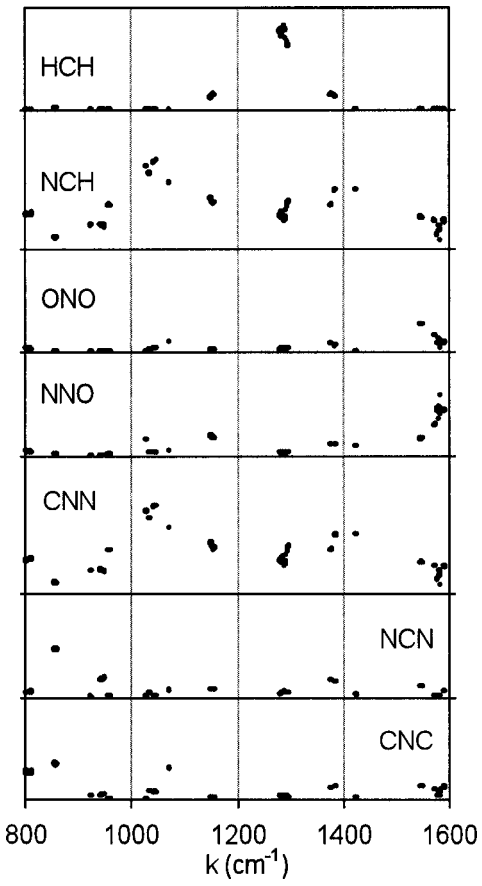

FIG. 9. Activities of bend angles in the normal modes of the crystal, wave number range from 800 to 1000 cm^{-1}. The apparent gaps in the data arise from the fact that there are no eigenmodes located in these data regions, see Figs. 3–6.

700 and 1600 cm^{-1}. This range includes various scissor, rock, and twist modes of the methyl groups. Neither HCH nor NCH shows activity at the lower frequencies; neither appears therefore of interest for any coupling of inter- and intramolecular degrees of freedom.

The nitro side groups can move under involvement of several bend angles. The ONO bending angles show activity in two places: A broad active range in ONO contributions between 609 and 688 cm^{-1} corresponds to the scissor modes of this group, similarly observed for the free molecule. The ONO contributions at 1590 cm^{-1} occur in conjunction with NN and NO stretch modes. The NNO bend angles will be associated with nitro rocking motions, found between 507 and 555 cm^{-1}, while a lesser contribution of this bend angle can be found also in other movements of this massive side group, such as the scissor modes. The CNN angle governs the relation of the NN bonds with respect to the ring; it is involved in all modes that challenge the ring to move without significant motion of the nitro group. Activity of this group is found in all methylene motions and ring modes. The CNC and NCN bend angles participate in all ring modes but generally do not show significant activity for other molecular modes. Figure 10 analyzes the four types of dihedral angles with respect to their activity in normal modes. Torsional and out-of-plane motions involve four atoms and belong to the group motions which are potentially interesting as couplings to lattice modes due to the frequency range in which they occur. The CNC–N wag angle would measure the out-of-plane motion of the nitro groups with respect to the plane defined by the CNC group in the ring to which it is attached (see sketch in Fig. 2). This wag angle is active in the ranges between 342 and 507 cm^{-1} (various ring modes with nitro rotations) and for the NO_2 scissor modes between 609 and 767 cm^{-1}. Some activity can also be found for the CH_2 twist modes around 950 cm^{-1}. In general, the nitro wagging motion is less pronounced than other dihedral motions of the nitro group; however, we would like to point out that this wagging nitro angle contributes to the symmetric methylene wag found around 426 cm^{-1}—a band which involves significant c.m translations of the whole molecule. The CNNO torsional angle dominates any twisting or rocking motions of the nitro group. The broad clusters of modes between 190 and 321 cm^{-1} correspond to rock and twist motions of the fairly massive nitro groups. As described below, some of these groups of modes involve lattice components and are therefore candidates for doorway modes. The CNCH torsional angle governs motions of the methyl group. The high activity of CNCH for the 1284 and 1294 bands is associated with the asymmetric CH_2 scissor modes. This dihedral group is actively involved in the methylene wagging modes, as well as some ring modes around the low 400 cm^{-1} range. Finally, there are six CNCN dihedral angles in the ring, which are significant for any ring mode, hence the broad contributions over the range of the spectrum. Lattice modes

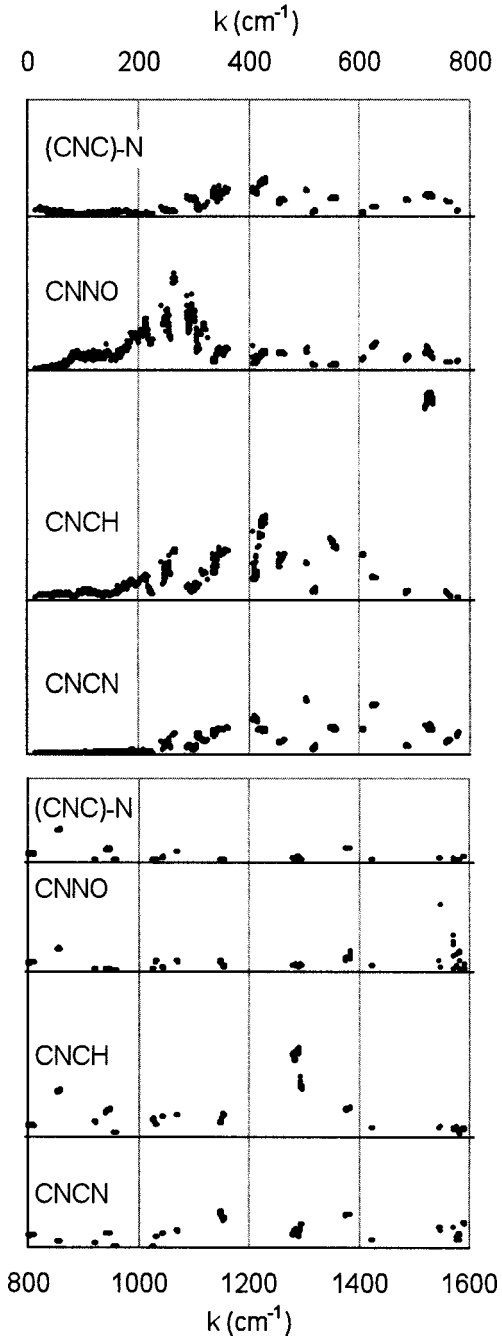

FIG. 10. Acitvies of the dihedral angles in the crystal modes. Included are the wag angle of the nitro groups (CNC–N) and three regular torsional angles. The figure is split into two panels for two wave-number ranges.

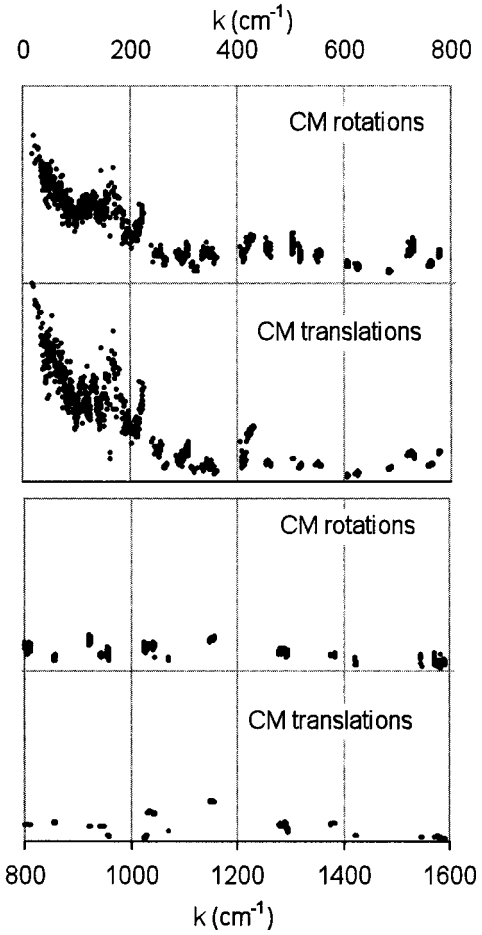

FIG. 11. Contributions of molecular C.M. translations and rotations to the crystal modes. The figure is split into two panels for two wave number ranges.

will invariably involve shifts in the c.m.s of molecules. Rotations of the molecular plane around an axis through the c.m. could also indicate contributions of the lattice to a normal mode. Figure 11 shows the resolution of c.m. rotations and translations of the molecules for the normal modes versus wave number. As expected, those primarily occur in a window below 500 cm^{-1}. Generally, the modes involve c.m. translations and rotations to approximately the same degree. A low level of c.m. activity can be observed throughout the spectrum and is associated with motion of massive parts of the molecule; such shifts do not constitute a lattice mode. Two features draw attention in the c.m. translations: The band at 223 cm^{-1} as well as the smaller band around 426 cm^{-1}. The first is associated with activity in the nitro dihedral activity, while the latter correlates with symmetric methylene wagging modes involving nitro wagging.

Addressing the question on how energy might be transferred from lattice degrees of freedom to intramolecular degrees of freedom, we examined the cross correlation between contributions of c.m. motion of the molecules and various internal degrees of freedom. In a correlation map, such as shown in Fig. 12, we seek modes that exhibit both c.m. motion as well as active internal motions. Modes lying close to the diagonal in such a plot would be likely candidates for doorway modes since they engage intra- as well as intermolecular degrees of freedom, and thus are able to transfer energy from lattice vibrations to the internal degrees of freedom of the molecules. On the other hand, modes lying close to either one of the axes will correspond to either purely lattice or molecular modes. Figure 12 shows correlations of the CNNO and CNC–N dihedral angles with molecular c.m. translations. The CNNO torsion is involved in any rotational motions of the nitro side groups. We find two groups of modes with high correlation. These clusters are located between 186 and 214 as well as between 214 and 220 cm^{-1}. Both of these bands involve vibrations of the chair-formed rigid ring structure, as well as a variety of motions of the nitro group. Figure 13 sketches two examples of typical mol-

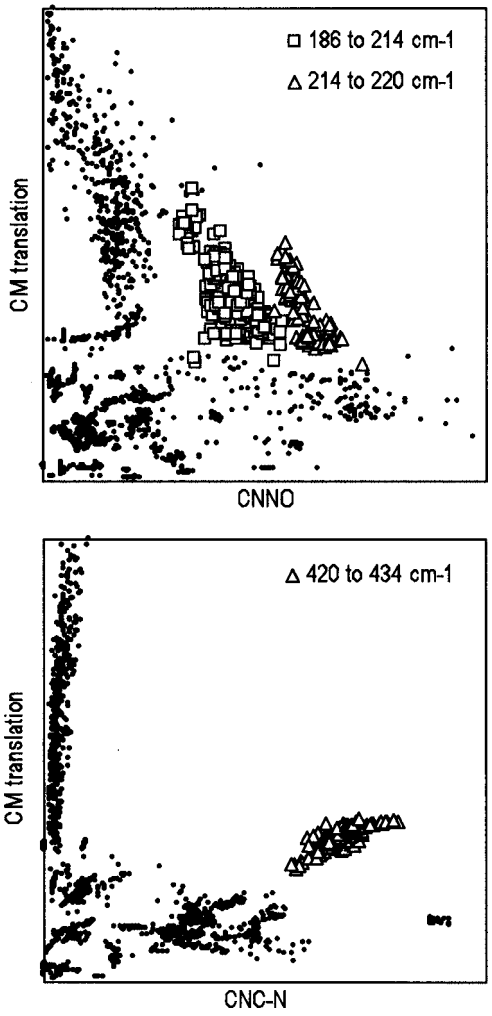

FIG. 12. Correlation maps of C.M. translations and internal dihedral motions for the normal modes. The first panel maps the correlation between molecule translations and the CNNO torsion. The second panel plots the molecule translation vs the wag angle CNC–N. Specially marked points correspond to the wave number ranges indicated.

ecule motions for the lower range (186–214 cm^{-1}). The ring motion is primarily a rotation around an axis normal to its average plane. Side group motion includes swaying and rocking of the nitro groups. In some cases, a twisting of the nitro groups occurs. The upper panel in Fig. 13 shows a molecule which exhibits all three observed motions in the 186–214 cm^{-1} band. The equatorial side group is swaying, while one of the axial groups is twisting (right). The left axial group is performing a kind of rocking motion, with minimal displacement of the heavy oxygen atoms. The band consists of modes with the distribution of these motions in various symmetric paces in the primitive cell. It appears that the common denominator of this mode is the ring rotation around an axis normal to the average plane of the ring. Examples of molecular motions in the higher band (214–220 cm^{-1}) are shown in Fig. 14. The ring rotation occurs primarily around an axis in its average plane, which leads to slightly different deformations of the nitro side groups. Twisting is less common in this group, but swaying and rocking of the nitro groups occur in all modes in this band. Comparable modes for the free molecule can be found

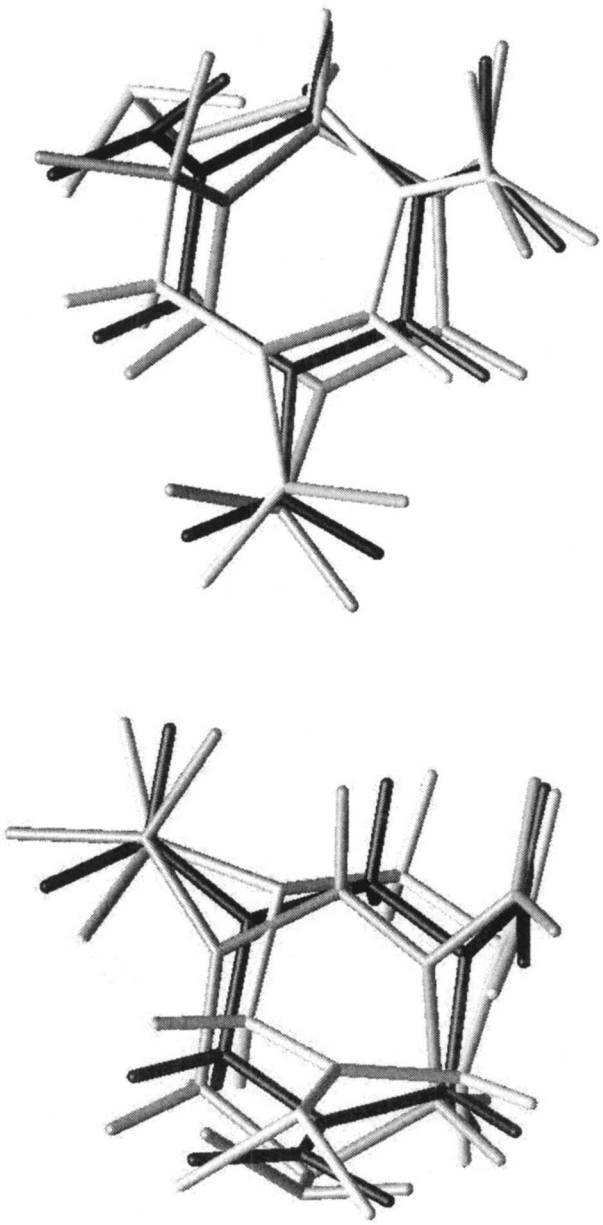

FIG. 13. Example for the molecule motion in the 186–214 cm^{-1} band. Equilibrium state is drawn in black.

at lower frequencies, around 80–170 cm^{-1}. When the molecules are embedded in the crystal, the higher constraints in its environment result in an increase in frequency, as well as different options with respect to symmetry.

In the second panel of Fig. 12, the out-of-plane angle of the nitro side groups is mapped with the c.m. translations of the molecules. The marked band corresponds to wave numbers between 420 and 434 cm^{-1}. These bands involve symmetric wagging of the CH_2 groups, as well as the associated distortions of the nitro groups. One example of a molecular motion is shown in Fig. 15. Not surprisingly, the CNCH torsional angles are very active in this range as well. Due to the molecular constraints, this motion cannot occur without affecting the wagging motion of at least one of the nitro groups. Equivalent modes for the free molecules[23] can be found around 300–400 cm^{-1}.

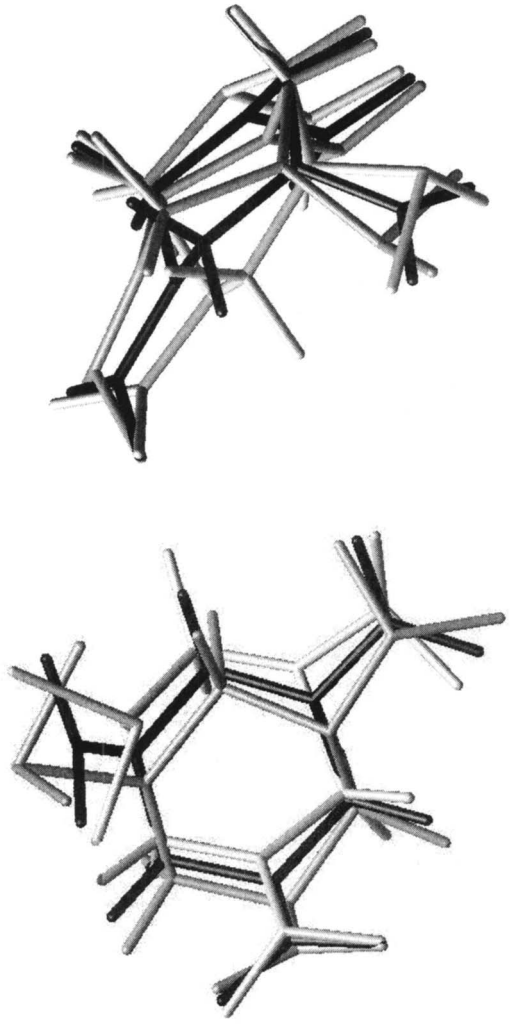

FIG. 14. Example for the molecule motion in the 214–220 cm^{-1} band. Equilibrium state is drawn in black.

While there are other normal modes which engage the nitro groups in dihedral distortions, those do not exhibit significant shifts in the c.m. of the molecules, and thus are not suited to transfer lattice momentum into intramolecular momentum. The bands identified above are potentially functional as doorway modes; if these bands engage, maybe due to shock, then rotations of the nitro side groups will occur. If enough energy is associated with this engagement, it is quite possible for nitro groups to detach from the molecule. However, it is likely that it may not be enough to single out a few bands of normal modes in order to understand detonation initiation. These bands are occupied thermally at room temperature; obviously other factors are needed in order to initiate bond breaking. Such factors may include anharmonic coupling, nonequilibrium occupation through shockwave, as well as crystal defects serving as focusing sites.

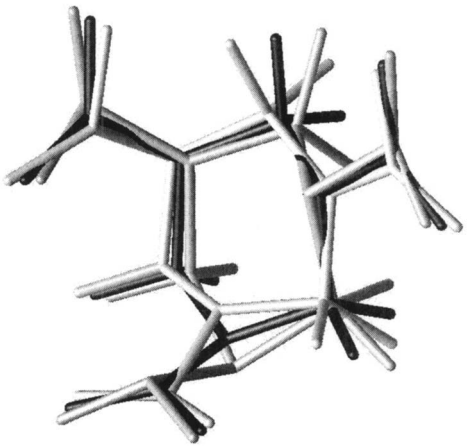

FIG. 15. Examples of molecule motions for the 420 and 434 cm^{-1} bands. Equilibrium state is drawn in black.

IV. SUMMARY

We have analyzed the normal mode spectrum of a computational model of α-RDX. The model includes intermolecular as well as intramolecular degrees of freedom, which allows establishing a complete picture of the interaction between lattice modes and molecular modes. The contributions of lattice modes and various types of internal degrees of freedom have been analyzed. We were successful in correlating motions involving the nitro groups and significant molecular c.m. motion. Such modes are able to aid in the transfer of energy from lattice motions, such as may occur in a shockwave, to intramolecular motions. While it is important to note that band positions will likely not quite agree with experimental values, we do want to emphasize that the existence of such combination modes in a computational model is a strong indication of their existence in the material. The doorway modes in our model are positioned in a wave number range between 186 and 220 cm^{-1} and to a lesser degree around 420–435 cm^{-1} and involve significant rotations of the nitro side groups. Further investigation of the influence of defects on the normal mode properties is needed.

ACKNOWLEDGMENTS

We thank Peter Politzer from the University of New Orleans for stimulating this project. The work was supported by a grant from the Dean of the Graduate School of the University of Minnesota, as well as by financial support from the University of Minnesota-Morris.

[1] F. P. Bowden and A. D. Yoffe, *Fast Reactions in Solids* (Butterworths, London, 1958).
[2] J. Sharma, J. C. Hoffsommer, D. J. Glover, C. S. Coffey, F. Santiago, A. Stolovy, and S. Yasuda, in *Shock Waves in Condensed Matter*, edited by J. R. Asay, R. A. Graham, and G. K. Straub (Elsevier, Amsterdam, 1984), p. 543.
[3] P. Maffre and M. Peyrard, Phys. Rev. B **45**, 9551 (1992).
[4] D. D. Dlott and M. D. Fayer, J. Chem. Phys. **92**, 3798 (1990); A. Tokmakoff, M. D. Fayer, and D. D. Dlott, J. Phys. Chem. **97**, 1901 (1993).
[5] Z. A. Dreger and Y. M. Gupta, J. Phys. Chem. B **111**, 3893 (2007).
[6] J. J. Haycraft, L. L. Stevens, and C. J. Eckhardt, J. Appl. Phys. **100**, 053508 (2006).
[7] S. M. Caulder, M. L. Buess, A. N. Garroway, and P. J. Miller, AIP Conf. Proc. **706**, 929 (2004).
[8] S. Ye, K. Tonokura, and M. Koshi, Combust. Flame **132**, 240 (2003).
[9] J. A. Ciezak, T. A. Jenkins, Z. Liu, and R. J. Hemley, J. Phys. Chem. A **59**, 111 (2007).

[10] N. Goto, H. Fujihisa, H. Yamawaki, K. Wakabayashi, Y. Nakayama, M. Yoshida, and M. Koshi, J. Phys. Chem. B **110**, 23655 (2006).
[11] R. J. Karpowicz and T. B. Brill, J. Phys. Chem. **87**, 2109 (1983).
[12] M. Rey-Lafon, C. Trinquecoste, R. Cavagnat, and M.-T. Forel, J. Chim. Phys. Phys.-Chim. Biol. **68**, 1533 (1971).
[13] M. R. Leahy-Hoppa, M. J. Fitch, X. Zheng, L. M. Hayden, and R. Osiander, Chem. Phys. Lett. **227**, 434 (2007).
[14] M. M. Kuklja, S. N. Rashkeev, and F. J. Zerilli, AIP Conf. Proc. **706**, 363 (2004).
[15] M. M. Kuklja, Appl. Phys. A: Mater. Sci. Process. **76**, 359 (2003).
[16] M. M. Kuklja, AIP Conf. Proc. **620**, 454 (2002).
[17] P. M. Agrawal, B. M. Rice, L. Zheng, and D. L. Thompson, J. Phys. Chem. B **110**, 26185 (2006).
[18] D. C. Sorescu, B. M. Rice, and D. L. Thompson, J. Phys. Chem. A **103**, 989 (1999).
[19] D. C. Sorescu, B. M. Rice, and D. L. Thompson, J. Phys. Chem. B **101**, 798 (1997).
[20] B. M. Rice and C. F. Chabalowski, J. Phys. Chem. A **101**, 8720 (1997).
[21] C. C. Chambers and D. L. Thompson, J. Phys. Chem. **99**, 15881 (1995).
[22] E. P. Wallis and D. L. Thompson, J. Chem. Phys. **99**, 2661 (1993).
[23] S. Boyd, M. Gravelle, and P. Politzer, J. Chem. Phys. **124**, 104508 (2006).
[24] C. S. Choi and E. Prince, Acta Crystallogr., Sect. B: Struct. Crystallogr. Cryst. Chem. **28**, 2857 (1972).
[25] I. F. Shishkov, L. V. Vilkov, M. Kolonists, and B. Rozsondai, Struct. Chem. **57**, 2 (1991).

AUTHOR QUERIES — 520838JCP

#1 Author-pls. confirm of change to ″with the force field of Agrawal et al.17″
#2 Au-Pls. confirm journal in Ref. 12
#3 Au-pls. insert footnote a in table
#4 Au-pls. insert footnotes a and b in table